Photoionization Microscopy

C. Nicole,* H. L. Offerhaus, and M. J. J. Vrakking
FOM Instituut voor Atoom en Molecuul Fysica (AMOLF), Kruislaan 407, 1098 SJ, Amsterdam, The Netherlands

F. Lépine and Ch. Bordas
Laboratoire de Spectrométrie Ionique et Moléculaire, UMR CNRS 5579,
Bâtiment A. Kastler, 43 Bvd. du 11 Novembre 1918, 69622 Villeurbanne Cedex, France
(Received 16 August 2001; published 15 March 2002)

We present the first experimental results of a technique called photoionization microscopy. Photoelectrons ejected in threshold photoionization of Xe are detected in a velocity map imaging apparatus, and interferences between various trajectories by which the electron moves from the atom to the detector are observed. The structure of the interference pattern, which contains the transverse component of the electronic wave function, evolves smoothly with the excess energy above the saddle point. The main observed features are interpreted within the framework of the semiclassical approximation.

DOI: 10.1103/PhysRevLett.88.133001 PACS numbers: 32.80.Fb, 07.81.+a, 32.60.+i, 32.80.Rm

Since the introduction of quantum mechanics, the direct observation of the wave function of an atomic system has been a physicist's dream. This goal, which for a long time could only be considered as a *gedanken* experiment, is now achievable thanks to improvements in photoelectron imaging. Until very recently, photoelectron imaging devices could visualize only the classical envelope of the wave function [1]. Only in 1996, with the development of the first photodetachment microscope, a direct observation of the oscillatory structure of a wave function became possible [2]. In this paper we present the first observation of an electronic wave function in atomic photoionization. Photoionization adds two additional features compared to photodetachment. Because of the more complicated electrostatic Coulomb + dc potential the trajectories are no longer parabolic, and above the saddle point to ionization the electron is optically excited to a continuum which is structured by a Stark manifold, which develops from the Rydberg level structure at zero field.

The principle of photodetachment or photoionization microscopy was introduced in the early 1980s in theoretical work [3,4]. The possibility of an experiment was discussed, where the two-dimensional (2D) flux of electrons escaping from a photodetachment or photoionization process in the presence of an electric field could be measured using a position-sensitive detector located at a macroscopic distance. On the detector the image formed by the electrons is the square modulus of the transverse component of the electronic wave function. Observed oscillatory patterns can be interpreted as a manifestation of interferences among various classical trajectories by which the electron moves from the atom to the detector. In photodetachment, only two trajectories interfere at each detector position and the observed structures can easily be interpreted based on analytical expressions of the phase accumulated along both trajectories [2,5]. In the case of photoionization the trajectories are considerably more complex [3,4,6], and one has to take into account the interference among an infinite number of classical paths. The simple trajectories relevant to the case of photodetachment, which are most conveniently analyzed in terms of the parabolic coordinates $\eta = r - z$ and $\xi = r + z$ (where r is the distance of the electron from the origin and z is the displacement along the electric field axis), are strongly perturbed, due to the Coulomb interaction between the ejected electron and the residual ion. Therefore, two-dimensional flux measurements are predicted to show a considerably more complex structure. Depending on the direction of emission, low energy photoelectrons will contribute to one of two distinct concentric structures, namely, a structure corresponding to electrons ejected down-field towards the bottleneck in the Coulomb + dc electric field potential (direct ionization) and one corresponding to electrons ejected away from the hole, which only ionize following further Coulomb interactions (indirect ionization). From the point of view of classical mechanics, direct ionization corresponds to trajectories where the number of oscillations along the ξ coordinate is zero, while indirect ionization corresponds to trajectories where the number of oscillations along the ξ coordinate is larger than zero.

In a recent paper [7] we published the first experimental observation of this phenomenon in imaging of the photoionization of atomic Xe. Observed images exhibited an outer ring, corresponding to the indirect ionization process, and an inner ring, corresponding to the direct ionization process, and clearly revealed how the indirect process dominates close to the saddle point, whereas the direct process dominates at higher excitation energies and above the field-free ionization limit. In the presence of an external electric field F the ionization threshold is lowered to the saddle-point energy $E_{sp} = -2\sqrt{F}$ (a.u.), above which a structured continuum exists which exhibits quasidiscrete Stark resonances [8]. For energies below approximately $0.775E_{sp}$ all classical trajectories have at least one turning point in the ξ coordinate when the electron moves from the atom to the detector, and therefore correspond

to indirect ionization, whereas direct trajectories without a turning point along the ξ coordinate become possible at energies above $0.775E_{sp}$, where furthermore their contribution rapidly becomes dominant [6]. Remarkable agreement was obtained between the experiment and the results of both classical and multichannel quantum defect calculations [9]. In this Letter we report on new observations in the imaging of photoionization of metastable $(6s[3/2]_{J=2})$ Xe atoms, made possible by a considerable improvement in our experimental apparatus [10]. In these new experiments the transverse component of the wave function is completely resolved, leading to the observation of extensive interference structures, as originally predicted in the theoretical work of Refs. [3] and [4]. These interferences can be understood by considering the accumulated phase of all trajectories and can provide an unprecedented microscopic view of the photoionization process.

Photoelectron imaging is based on the projection of electrons formed in laser photoionization or photodetachment onto a 2D position-sensitive detector, consisting of a microchannel plate + phosphorscreen detector in combination with a camera system. The recorded images can be used to recover the original three-dimensional (3D) velocity and angular distribution of the electrons. By use of a velocity map imaging geometry [11], it is possible to project electrons with one unique initial 3D velocity vector originating from a source volume with a diameter of 1–2 mm to a spot with a diameter of approximately 100 μm. However, the typical size of the images recorded near the ionization threshold and of the interference fringes is extremely small: In the experiments in Ref. [7] (using a flight length of 50 cm and an extraction field strength of 170 V/cm) the overall image size was on the order of 1 mm, and the experimental conditions were such that the fringe spacing was substantially smaller than 100 μm. Moreover, in these experiments, the number of possible fringes, which in a hydrogenic system would correspond to the parabolic quantum number n_ξ of the quasidiscrete Stark resonances [3,4], was difficult to estimate and potentially very large. Therefore, we have developed an electrostatic magnifying lens, which is mounted halfway between the ionization region and the 2D position-sensitive detector (i.e., in the time-of-flight tube of the velocity map imaging detector), that allows a magnification of an image formed at the entrance to the lens by a factor as large as 20 without deterioration of the image quality and, above all, without perturbation of the pattern of the interferogram [10]. With this magnifying lens, images can be recorded with a radius of several mm in a kinetic energy domain and dc electric field regime, where (i) the number of fringes is not too high, and (ii) the continuum Stark structure can be resolved. Because of the bandwidth of our laser (a Quanta-Ray PDL-3, with a 0.07 cm^{-1} bandwidth in the visible), condition (ii) was fulfilled only for $F > 500$ V/cm. Working at a somewhat smaller field of 300 V/cm allowed us to obtain more resolved interference fringes, even though in that case the respective contribution of the continuum and of the resonances is more difficult to distinguish. At field strengths below 150 V/cm the quality of our imaging setup is degraded, possibly as a result of small residual magnetic fields. As before, the metastable Xe atoms were formed in an electron impact source.

Figure 1(a) shows an experimental image which was recorded with the new instrument at a field strength of 320 V/cm in the extraction region [12] and with the laser (one-photon excitation near 325 nm, linear polarization parallel to the plane of the detector) tuned about 13.8 cm^{-1} above the saddle-point energy. An interference pattern is clearly observed, which shows five radii, where a constructive interference takes place. The interference can also be observed in Fig. 1(b), which shows the radial probability distribution $P(R)$ derived from the image, according to $P(R) = \int P(R, \alpha) R \, d\alpha$, where $P(R, \alpha)$ represents the intensity distribution in the image in polar coordinates R and α. Images were recorded similar to Fig. 1, while scanning the ionization laser frequency between the saddle point and the zero-field ionization threshold at field strengths of 320 and 615 V/cm, in the latter case allowing measurements both on pronounced quasidiscrete Stark resonances and between them. The most striking result of these measurements is the smooth evolution of the interference pattern.

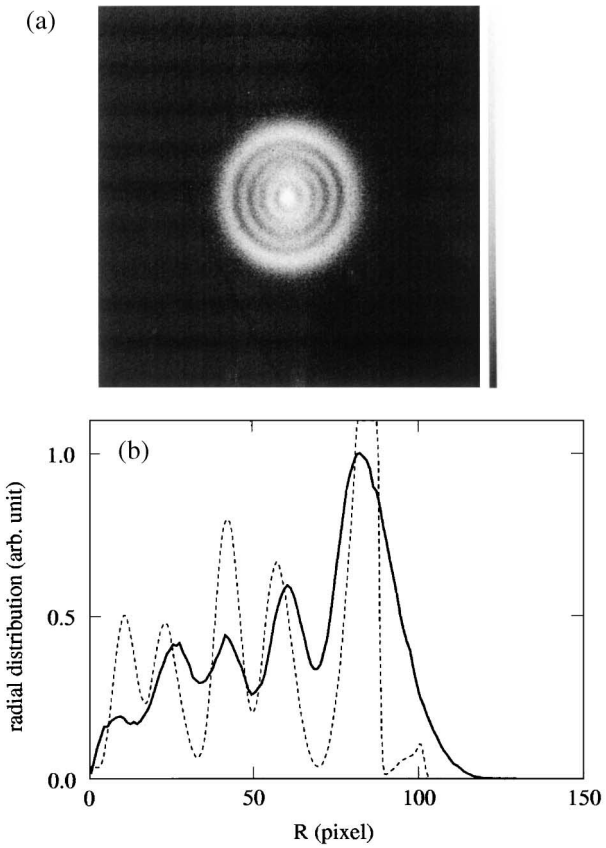

FIG. 1. (a) Experimental photoelectron image recorded in a dc electric field of 320 V/cm, by exciting metastable Xe $6s[3/2]_{J=2}$13.8 cm^{-1} above the saddle point with a laser (λ_{vac} = 326.05 nm) polarized parallel to the plane of the detector, and along the vertical axis. (b) Comparison of the experimental (solid line) and theoretical (dashed line) radial probability distributions $P(R)$ of the image.

Over the entire excitation range the number of dark fringes increases smoothly as a function of the excess energy with respect to the saddle-point energy, and — to a first approximation — the quasidiscrete Stark resonances affect only the amplitude of the modulation of the various fringes, but not the fringe position. Note that the angular distribution is also extremely sensitive to being on or off resonance but this is mainly connected to the excitation process and will not be discussed further here. Thus, the experiment shows unambiguously that — in contrast with predictions in the literature pertaining to atomic hydrogen [3,4] — interferograms for the photoionization of a nonhydrogenic atom like Xe are *not* dominated by the transverse nodal structures of well-defined quasidiscrete Stark resonances but can be almost completely understood on the basis of continuum background contributions. In other words, the system behaves as if the electrons were ejected isotropically with respect to the external electric field.

As in Ref. [7], the current experiments clearly reveal the presence of both a direct and an indirect ionization path. Figure 2(a) shows an image which was recorded at a field of 320 V/cm with the laser tuned about 27.8 cm^{-1} above the saddle-point energy. The radial probability distribution $P(R)$ derived from the image is shown in Fig. 2(b). The image shows the onset of the appearance of an intense central portion, which corresponds to direct ionization, surrounded by the contribution due to indirect ionization. When the measurements are extended to higher energy, an onset of interference structures in the inner region is observed which is qualitatively similar to the onset of the interference structures in the indirect ionization component at lower energies. These structures arise predominantly from the interference on the detector between two trajectories corresponding to direct ionization, similar to the case of photodetachment. We note that — unlike photodetachment — the interference in the inner region is complicated by a beat structure arising from the interference between direct and indirect trajectories.

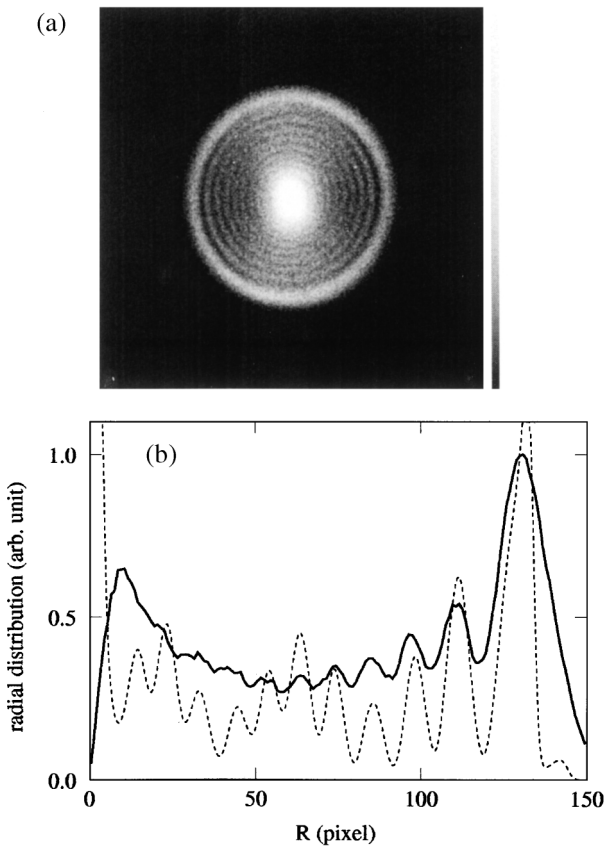

FIG. 2. (a) Experimental photoelectron image recorded in a dc electric field of 320 V/cm, by exciting metastable Xe $6s[3/2]_{J=2}27.8$ cm^{-1} above the saddle point with a laser (λ_{vac} = 325.90 nm) polarized parallel to the plane of the detector, and along the vertical axis. The bright central and weaker outer portions of the image correspond to electrons which ionize directly and indirectly, respectively. (b) Comparison of the experimental (solid line) and theoretical (dashed line) radial probability distributions $P(R)$ of the image.

In order to analyze the observed interference structures, we have performed semiclassical trajectory calculations. These trajectory calculations are similar to the ones reported earlier [6], except that now the phase integral (or reduced action) along the classical path is evaluated using expressions given in Refs. [3] and [4]. Our treatment is strictly limited to the semiclassical approximation, i.e., we do not introduce any correction to the phase to account for the failure of the semiclassical approximation when the momenta p_ξ or p_η vanish. In addition, we neglect the contribution of tunneling integrals. The total electron flux on the detector was calculated by summing the wave function amplitudes of all electron trajectories on the detector including the reduced action S_η and S_ξ accumulated along the η and ξ coordinates, respectively, according to

$$j(R_i) = \sum_j [I(\theta_{ij})\,(\sin\theta_{ij}\,d\theta_{ij})/(R_i\,dR_i)]^{1/2} \times \exp\{i[S_\eta(\theta_{ij}) + S_\xi(\theta_{ij})]\},$$

where θ_{ij} represent all ejection angles which lead to the detection of the electron at radius R_i. From this, the radial probability distribution $P(R)$ is obtained according to $P(R) = R|j(R)|^2$. We assume an isotropic initial electron angular distribution throughout all calculations [13], which means that we account only for the so-called background contribution as defined in Refs. [3] and [4]. Figures 1(b) and 2(b) compare the semiclassical and experimental radial probability distributions $P(R)$. The agreement between experiment and theory is remarkable given the assumptions made. In fact, most discrepancies are likely attributable to the semiclassical approximation itself. A fully quantum mechanical calculation, taking accurately into account the optical excitation and the importance of nonzero quantum defects, would undoubtedly lead to a better quantitative agreement. These quantum calculations will be performed in the future. Qualitatively, however, the overall features are already understood in the semiclassical approximation.

The comparison between the experimental results and the semiclassical simulations are further illustrated in Fig. 3. Here the position of dark fringes in the experimen-

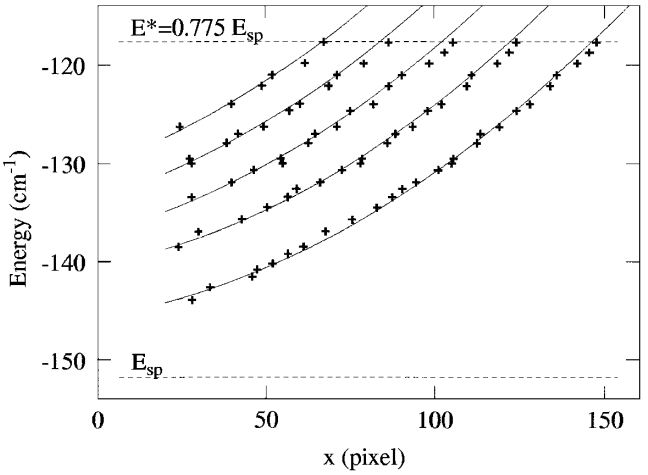

FIG. 3. Comparison of the experimental (+) and theoretical (solid lines) position of dark fringes in the images, for images recorded in a dc electric field of 615 V/cm. The excellent agreement between the experimental and theoretical results illustrates that the experimental results can be almost completely understood by considering direct excitation to the continuum, and that quasidiscrete Stark resonances do not affect the fringe positions. The saddle-point energy E_{sp} as well as the energy above which direct trajectories exist ($E^* \approx 0.775 E_{sp}$) are indicated by dashed lines.

tal and the semiclassical images is shown as a function of the excitation energy above the saddle point, for a field strength of 615 V/cm. The comparison shows convincingly how the interferograms can be almost completely understood on the basis of the continuum background contributions calculated in the semiclassical model. Quasidiscrete Stark resonances, though clearly revealed in the wavelength dependence of the photoionization efficiency, hardly manifest themselves in the fringe positions. The number of dark fringes observed is governed by the photoelectron excess kinetic energy above the saddle-point energy and the strength of the electric field, rather than the (approximate) transverse parabolic quantum numbers of the quasidiscrete Stark states. We note that we have clear experimental evidence that the ratio of the direct and indirect contribution in the image is extremely sensitive to being on or off resonance. On resonance, the contribution of indirect trajectories tends to be larger than off resonance. This is consistent with the classical picture of Stark resonances having a wave function localized in the up-field region of the potential.

In conclusion these results demonstrate unambiguously that photoionization microscopy allows a deeper insight into ionization processes in an external electric field. Interference patterns corresponding to the transverse component of the Stark momentum wave function have been observed for the first time. The background contribution is clearly dominant for a nonhydrogenic system such as xenon. Clearly, similar experiments on atomic hydrogen are desirable.

Beyond a direct observation of the electronic wave function, photoionization microscopy provides a unique model system to access given components of the wave function (e.g., parts of the wave function corresponding to direct vs indirect ionization). In the future we would like to investigate to what extent photoionization microscopy allows the construction of an atomic-size interferometer, enabling the direct observation of the influence of an external perturbation such as a magnetic field or the presence of neighboring ions.

This work is part of the research program of FOM (Fundamental Research on Matter); which is subsidized by the NWO (Netherlands Organization for the Advancement of Research). C. N. acknowledges the European Community for receipt of a Marie-Curie grant. C. B., F. L., and M. V. acknowledge the support of the Van Gogh program.

*Present address: Philips Electronics Nederland B.V., Prof. Holstlaan 4, 5656 AA, Eindhoven, The Netherlands.

[1] (a) A. J. R. Heck and D. W. Chandler, Annu. Rev. Phys. Chem. **46**, 335 (1995); (b) C. Bordas, F. Paulig, H. Helm, and D. L. Huestis, Rev. Sci. Instrum. **67**, 2257 (1996).

[2] C. Blondel, C. Delsart, and F. Dulieu, Phys. Rev. Lett. **77**, 3755 (1996).

[3] Yu. N. Demkov, V. D. Kondratovich, and V. N. Ostrovsky, Pis'ma Zh. Eksp. Teor. Fiz. **34**, 425 (1981) [JETP Lett. **34**, 425 (1981)].

[4] (a) V. D. Kondratovich and V. N. Ostrovsky, J. Phys. B **17**, 1981 (1984); (b) J. Phys. B **17**, 2011 (1984); (c) J. Phys. B **23**, 21 (1990); (d) J. Phys. B **23**, 3785 (1990).

[5] (a) C. Bracher, W. Becker, S. A. Gurwitz, M. Kleber, and M. S. Marinov, Am. J. Phys. **66**, 38 (1998); (b) C. Blondel, C. Delsart, F. Dulieu, and C. Valli, Eur. Phys. J. D **5**, 207 (1999); (c) C. Blondel, S. Berge, and C. Delsart, Am. J. Phys. **69**, 810 (2001).

[6] Ch. Bordas, Phys. Rev. A **58**, 400 (1998).

[7] C. Nicole, I. Sluimer, F. Rosca-Pruna, M. Warntjes, M. J. J. Vrakking, C. Bordas, F. Texier, and F. Robicheaux, Phys. Rev. Lett. **85**, 4024 (2000).

[8] R. R. Freeman, N. P. Economou, G. C. Bjorklund, and K. T. Lu, Phys. Rev. Lett. **41**, 1463 (1978).

[9] F. Texier (to be published).

[10] H. L. Offerhaus, C. Nicole, F. Lépine, C. Bordas, F. Rosca-Pruna, and M. J. J. Vrakking, Rev. Sci. Instrum. **72**, 3245 (2001).

[11] A. T. J. B. Eppink and D. H. Parker, Rev. Sci. Instrum. **68**, 3477 (1997).

[12] In velocity map imaging the extraction field is inhomogeneous and the field strength is difficult to derive accurately from the voltages applied to the repeller and extractor electrodes. Therefore, the calibration of the field strengths was first estimated from the voltage readings, and then refined by comparing the experimental results to the result of the semiclassical simulations.

[13] Experimentally, rapid variations were observed in the angular distributions of the images, accompanied by a gradual rise of the β parameter from 0.3 to 0.7.